Polarization transfer and spin response functions of the $^2\mathrm{H}(\vec{p},\vec{n})$ reaction at 345 MeV

T. Wakasa,[1,*] H. Sakai,[2,3] M. Ichimura,[4] K. Hatanaka,[5] M. B. Greenfield,[6] M. Hatano,[2] J. Kamiya,[7] H. Kato,[2] Y. Maeda,[2] H. Okamura,[8] T. Ohnishi,[3] H. Otsu,[9] K. Sekiguchi,[3] K. Suda,[10] A. Tamii,[5] T. Uesaka,[11] T. Yagita,[1] and K. Yako[2]

[1]*Department of Physics, Kyushu University, Higashi, Fukuoka 812-8581, Japan*
[2]*Department of Physics, The University of Tokyo, Bunkyo, Tokyo 113-0033, Japan*
[3]*The Institute of Physical and Chemical Research, Wako, Saitama 351-0198, Japan*
[4]*Faculty of Computer and Information Sciences, Hosei University, Koganei, Tokyo 184-8584, Japan*
[5]*Research Center for Nuclear Physics, Osaka University, Ibaraki, Osaka 567-0047, Japan*
[6]*Division of Natural Science, International Christian University, Mitaka, Tokyo 181-8585, Japan*
[7]*Accelerator Group, Japan Atomic Energy Research Institute, Tokai, Ibaraki 319-1195, Japan*
[8]*Cyclotron and Radioisotope Center, Tohoku University, Sendai, Miyagi 980-8578, Japan*
[9]*Department of Physics, Tohoku University, Sendai, Miyagi 980-8578, Japan*
[10]*Department of Physics, Saitama University, Saitama, Saitama 338-8570, Japan*
[11]*Center for Nuclear Study, The University of Tokyo, Bunkyo, Tokyo 113-0033, Japan*

(Received 14 January 2004; published 2 April 2004)

Differential cross sections and a complete set of polarization observables have been measured in the quasielastic $^2\mathrm{H}(p,n)$ reaction at a bombarding energy of 345 MeV and laboratory scattering angles of 16°, 22°, and 27°. The data are compared with plane-wave impulse approximation calculations employing an optimal factorization approximation. The agreement between the experimental and theoretical results validates these approximations in the present momentum- and energy-transfer regions. The experimental spin-longitudinal and spin-transverse response functions, R_L and R_T, respectively, are deduced from the data. The obtained R_T is consistent with that obtained from the quasielastic electron scattering. The theoretical calculations with the Reid soft core potential give good descriptions for R_L and R_T, whereas the latter is slightly underestimated around the quasielastic peak.

DOI: 10.1103/PhysRevC.69.044602 PACS number(s): 25.40.Kv, 24.70.+s, 25.10.+s

I. INTRODUCTION

In this article, we present the differential cross sections and a complete set of polarization observables of the quasielastic $^2\mathrm{H}(p,n)$ reaction at the proton incident energy $T_p = 345$ MeV, and laboratory scattering angles of 16°, 22°, and 27° corresponding to momentum transfers $q_{\mathrm{lab}} \simeq 1.2, 1.7$, and 2.0 fm^{-1}. The data obtained at $T_p > 100$ MeV is of particular interest since it enables the investigation of the reaction mechanism of the (p,n) reaction leading to the continuum, as well as provides a testing ground for the theoretical calculations of spin-isospin structures of nuclei [1–3].

One of the unique points of the $^2\mathrm{H}(p,n)$ reaction is that the relevant response functions can be rigorously calculated. Thus we compare our data with plane-wave impulse approximation (PWIA) calculations [4], employing the optimal factorization approximation [5–8] to access the accuracy of these approximations. Furthermore, the agreement between the experimental and theoretical results measures the dominance of the one-step quasielastic process assumed in the calculations. Note that these approximations, together with an effective neutron number approximation for the absorption, have been also used to analyze complete sets of polarization observables for quasielastic (p,n) reactions [2,8–12].

The differential cross sections and a complete set of polarization observables are used to separate the cross sections into nonspin, spin-longitudinal, and two spin-longitudinal polarized cross sections. The spin-longitudinal and spin-transverse polarized cross sections are used to extract the spin-longitudinal R_L and spin-transverse R_T response functions, respectively. The observed R_T is compared with the corresponding R_T obtained via the quasielastic electron scattering. The energy spectra of R_L and R_T are compared with theoretical calculations using the Reid soft core potential.

II. EXPERIMENTAL METHODS

The experiment was performed at the Neutron Time-Of-Flight (NTOF) facility [13] at the Research Center for Nuclear Physics (RCNP), Osaka University. The experimental arrangement and procedure were similar to those reported previously [13–15]. In the following, therefore, we present a brief description of the detector system and discuss experimental details relevant to the present experiment.

A. Polarized proton beam

The High Intensity Polarized Ion Source (HIPIS) at RCNP [16] was used to produce the polarized proton beam. The nuclear polarization state was cycled between the normal and reverse states (e.g., between "up" and "down" at the exit of the AVF cyclotron) by selecting rf transitions. During the data acquisition, the beam polarization direction was reversed every 10 sec in order to minimize geometrical false-asymmetries. The polarized proton beam from HIPIS was

*Email address: wakasa@phys.kyushu-u.ac.jp: http://www.kutl.kyushu-u.ac.jp/~member/wakasa

injected into the AVF cyclotron and was accelerated up to $T_p = 59.7$ MeV. The rf frequency of the AVF cyclotron was 16.244 MHz, which corresponded to a beam pulse period of 61.6 ns. One out of nine beam pulses was selected before injection into the Ring cyclotron, which then yielded a beam pulse period of 554.1 ns. This pulse selection reduces the wraparound of slow neutrons from preceding beam pulses. The pulse-selected beam was accelerated up to $T_p = 345$ MeV in the Ring cyclotron. The single-turn extraction was maintained during the measurement in order to keep the beam pulse period. Multiturn extracted protons were less than 0.5 % of single-turn extracted ones.

B. Proton spin precession magnets

Superconducting solenoid magnets, SOL1 and SOL2, located in the injection line from the AVF to Ring cyclotrons, were used to precess the proton spin direction. Each magnet can rotate the direction of the polarization vector from the normal $\hat{N}$ into sideways $\hat{S}$ directions. These two magnets are separated by a bending angle of 45°, thus they can deliver the beam to the Ring cyclotron with two different directions of the polarization vector in the horizontal plane. The spin precession angle in this bending magnet is about 85.8° for 59.7 MeV protons. Thus the longitudinal $\hat{L}$ and sideways $\hat{S}$ polarized proton beams can be provided at the exit of SOL2 by using the SOL1 and SOL2 magnets, respectively.

C. Beam line polarimeters

The beam from the Ring cyclotron was transported to the neutron experimental hall through the $N\phi$ beam line. All components (S,N,L) of the beam polarization just upstream of the target were continuously monitored with two sets of beam line polarimeters, BLP1 and BLP2. BLP1 is positioned at the $N\phi$ beam line, and BLP2 is located in the neutron experimental hall. These two polarimeters are separated with a bending angle of 98°, allowing simultaneous determination of all of the components of the polarization vector.

Each polarimeter consists of four pairs of conjugate-angle plastic scintillators. The $\vec{p}+p$ elastic scattering was used as the analyzing reaction, and a self-supporting CH_2 target with a thickness of 1.1 mg/cm^2 was used as the hydrogen target. The elastically scattered and recoiled protons were detected in kinematical coincidence with a pair of scintillators.

The analyzing powers of beam line polarimeters contain the contribution from the quasielastic $^{12}C(\vec{p},2p)$ reaction, whose analyzing power might be different from that for the free *pp* scattering. The effective analyzing powers, including this contribution, were calibrated as described in detail in Ref. [15]. The resulting value at $T_p = 345$ MeV is 0.430 ± 0.003, where the uncertainty is systematic.

The averaged magnitude of the beam polarization was 0.70 for each polarization state, with a typical magnitude difference of about 0.01 between the two different states. This difference is comparable to the statistical accuracy of the beam polarization measurement. Thus we used the averaged value to deduce the polarization observables.

D. Beam swinger system and targets

Targets for the $(\vec{p},\vec{n})$ reaction were placed in the beam swinger system, which consists of two 45° bending magnets. The reaction angle was varied by repositioning a target along the beam trajectory inside the system, while the position of NPOL2 was fixed along a 100 m time-of-flight (TOF) tunnel. Protons downstream of the target were swept by the beam swinger magnets into a graphite beam stop (Faraday cup) from which the integrated beam current was measured. Typical beam currents were 10 and 50 nA for the cross section and D_{ij} measurements, respectively.

The data for the $^2H(\vec{p},\vec{n})$ reaction were deduced from the cross section weighted difference between the CD_2 and ^{12}C results. Relatively thin targets with areal densities of 222 mg/cm^2 for CD_2 and 172 mg/cm^2 for ^{12}C were used for the measurement of cross sections and analyzing powers so as to minimize loss in the swinger magnets, which is essential in order to accurately determine differential cross sections as described below. In the measurement of D_{ij}, thicker targets with areal densities of 662 mg/cm^2 for CD_2 and 682 mg/cm^2 for ^{12}C were required in order to achieve sufficient statistical accuracy for D_{ij} values.

E. Neutron spin rotation magnet and NPOL2

A dipole magnet (NSR magnet) located at the entrance of the TOF tunnel was used to precess the neutron polarization vector from the longitudinal $\hat{L}'$ into normal $\hat{N}'$ directions so as to make the longitudinal component measurable with NPOL2. In the measurement of the longitudinal component of the neutron polarization, the NSR magnet was excited so that the precession angle for the neutron corresponding to the quasielastic peak was 90°. Corrections for the over- and underprecessions to the lower and higher energy neutrons were performed to account for the mixing between the longitudinal and normal components.

Neutrons were detected with the neutron detector/polarimeter NPOL2 at the end of the 100 m flight path. The NPOL2 system [15] consists of six planes of two-dimensionally position-sensitive scintillation detectors: four liquid scintillators BC519 and two plastic scintillators BC408. The BC519 with a high hydrogen-to-carbon ratio of 1.7 was used since the neutron polarization is determined via the $\vec{n}+p$ scattering in the scintillator material. Each of the six neutron detectors has an effective detection area of approximately 1 m^2 with a thickness of 0.1 m. Thin plastic scintillation detectors in front of each neutron detector were used to tag charged particles.

Incident neutron energies were determined by the TOF to the given neutron detector with respect to a cyclotron rf signal. A prominent γ ray from the π^0 decay in the target provides a time reference for the absolute timing calibration. Then, the transitions to discrete states with known reaction *Q* values were used to determine the incident beam energy. The beam energy was thus determined to be $T_p = 345 \pm 1$ MeV for the measurement at $\theta_{lab} = 16°$ and 27°, whereas it was $T_p = 346 \pm 1$ MeV for the measurement at $\theta_{lab} = 22°$. The full width at half-maximum energy resolutions are about 2 and

3 MeV for the cross sections and D_{ij} measurements, respectively.

III. DATA REDUCTION

A. Polarization observables

A complete set of polarization observables A_y, P, and $D_{ij}(i=S',N',L',j=S,N,L)$ relates the three orthogonal components of the outgoing neutron polarization $\mathbf{p}'=(p'_S,p'_N,p'_L)$ to those of the incident proton polarization $\mathbf{p}=(p_S,p_N,p_L)$ through

$$\begin{pmatrix} p'_{S'} \\ p'_{N'} \\ p'_{L'} \end{pmatrix} = \left[\begin{pmatrix} D_{S'S} & 0 & D_{S'L} \\ 0 & D_{NN} & 0 \\ D_{L'S} & 0 & D_{L'L} \end{pmatrix} \begin{pmatrix} p_S \\ p_N \\ p_L \end{pmatrix} + \begin{pmatrix} 0 \\ P \\ 0 \end{pmatrix} \right] \frac{1}{1+p_N A_y}. \tag{1}$$

This relation involves all the polarization observables allowed by parity conservation. The sideways S, normal N, and longitudinal L coordinates are defined in terms of the proton and neutron momenta, $\hat{\mathbf{k}}_{\rm lab}$ and $\hat{\mathbf{k}}'_{\rm lab}$, in the laboratory frame as $\hat{\mathbf{L}}=\hat{\mathbf{k}}_{\rm lab}$, $\hat{\mathbf{L}}'=\hat{\mathbf{k}}'_{\rm lab}$, $\hat{\mathbf{N}}=\hat{\mathbf{N}}'=(\mathbf{k}_{\rm lab}\times\mathbf{k}'_{\rm lab})/|\mathbf{k}_{\rm lab}\times\mathbf{k}'_{\rm lab}|$, $\hat{\mathbf{S}}=\hat{\mathbf{N}}\times\hat{\mathbf{L}}$, and $\hat{\mathbf{S}}'=\hat{\mathbf{N}}'\times\hat{\mathbf{L}}'$.

The analyzing power A_y, the induced polarization P, and the polarization transfer coefficient D_{NN} were measured with the N-type beam. The other polarization transfer coefficients, $D_{S'S}$, $D_{L'S}$, $D_{S'L}$, and $D_{L'L}$, were obtained from the measurements with two different proton beams polarized in the L-S plane. The direction of the proton polarization vector in this plane can be rotated by about 90° by using SOL1 and SOL2, therefore, the efficiency of measuring these D_{ij} is almost the same as that with pure S- and L-type beams.

B. Neutron detection efficiency

The relation between the observed neutron yield $N_{\rm obs}$ and the double differential cross section $\sigma_{\rm lab}$ is given by

$$\sigma_{\rm lab}=\frac{N_{\rm obs}}{\mathcal{I}\rho\Delta\Omega\epsilon T f_{\rm live}}, \tag{2}$$

where $\mathcal{I}$ is the number of incident protons, ρ the target thickness, $\Delta\Omega$ the solid angle subtended by NPOL2, ϵ the intrinsic neutron detection efficiency, T the transmission factor along the flight path in the air, and $f_{\rm live}$ the detector live fraction.

Since it is very difficult to obtain the ϵ and T values independently, we measured the product of these two values by using the neutrons from the zero-degree $^7{\rm Li}(p,n)^7{\rm Be}({\rm g.s.}+0.43\ {\rm MeV})$ reaction, which has a constant center-of-mass cross section of $\sigma_{\rm c.m.}=27.0\pm0.8$ mb/sr over the wide incident energy range of $T_p=80-795$ MeV [17]. The independent measurements [15] were performed at the incident beam energy range of $T_p=146-392$ MeV, which covers the neutron energy range necessary for the present data analysis. It is found that the neutron detection efficiencies ϵT are almost independent of neutron kinetic energy in this region, with a value of 0.15 ± 0.01 by combining all of the six neutron detectors [15]. The additional measurement for this reaction at $T_p=345$ MeV was made during the present measurement, and the detection efficiency was determined to be 0.14 ± 0.01 where the uncertainty mainly comes from the uncertainties both in the ^{7}Li cross section (3%) and the thickness of the ^{7}Li target (3%). The small discrepancy between the present and previously measured efficiencies seems to be due to different detection thresholds of the neutron detectors. Thus we used the present value of 0.14 as the detection efficiency for all neutron kinetic energies.

C. Effective analyzing powers

The neutron polarization is analyzed by using the $\vec{n}+p$ scattering in a neutron detector of NPOL2, and doubly scattered neutrons or recoil protons are detected with the following neutron detector. Time, position, and pulse-height information from both detectors are used to kinematically select the $\vec{n}+p$ events. The time resolution of neutron detectors is about 0.5 ns, and the position resolutions, which are location dependent, are about 6–10 and 4–8 cm for liquid and plastic scintillators, respectively. Both the normal N' and sideways S' components of the neutron polarization are measured simultaneously with the azimuthal distribution of the $\vec{n}+p$ events.

The effective analyzing powers of NPOL2 were measured with polarized neutrons produced by the zero-degree $^2{\rm H}(\vec{p},\vec{n})pp$ reaction at $T_p=146-392$ MeV, and the results are described in detail in Ref. [15]. For example, effective analyzing powers of NPOL2 at $T_n=291$ MeV and their statistical uncertainties are 0.223 ± 0.010 and 0.132 ± 0.004 for $(\vec{n},n)$ and $(\vec{n},p)$ channels, respectively. The correction for the energy dependence of the effective analyzing powers has been applied to the present data.

D. Normalizations for the previous data

The differential cross sections for (p,n) reactions on ^{2}H and ^{12}C at $T_p=345$ MeV and $\theta_{\rm lab}=22°$, which were already measured in our previous measurement [2], were herein found to be systematically smaller than the corresponding previous data. The difference is most likely due to the beam loss in the swinger magnets caused by the multiple scattering effects in the previously used thicker targets. In this measurement, we used appropriately thin targets with thicknesses of 222 and 172 mg/cm^2 for CD_2 and ^{12}C, respectively, in order to reduce the beam loss. Measurements with thinner and empty targets were performed, and the beam loss is found to be less than 1% in the present measurement. Measurements for (p,n) reactions on ^{6}Li, ^{40}Ca, and ^{208}Pb were also performed with thinner targets compared with those in Ref. [2], and the normalization factors for the cross sections in Ref. [2] are determined to be 0.77, 0.82, and 0.75 for ^{6}Li, ^{40}Ca, and ^{208}Pb, respectively.

IV. RESULTS AND ANALYSIS

A. Observables for $^2{\rm H}(\vec{p},\vec{n})$

Observables for the $^2{\rm H}(\vec{p},\vec{n})$ reaction were obtained by means of a cross section weighted subtraction of the

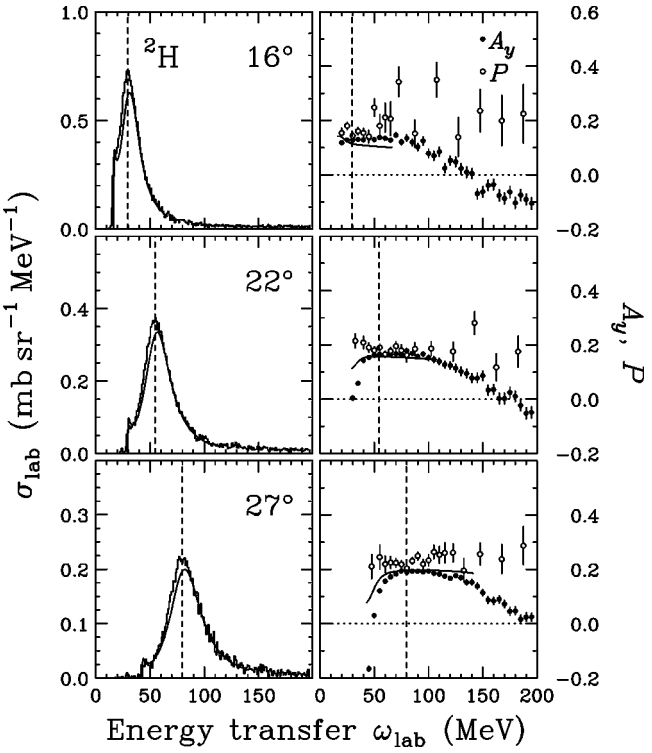

FIG. 1. Cross section, analyzing power, and induced polarization spectra for the ^{2}H(p,n) reaction at T_p=345 MeV and θ_{lab} =16°,22°, and 27°. The cross sections (left panels) and analyzing powers (right panels) are binned in 1 and 5 MeV steps, respectively. The induced polarizations (right panels) are binned in 5–20 MeV steps, depending on their statistics. The vertical dashed lines mark the energy transfer for the free *np* scattering. The solid curves are the PWIA predictions with the optimal factorization approximation.

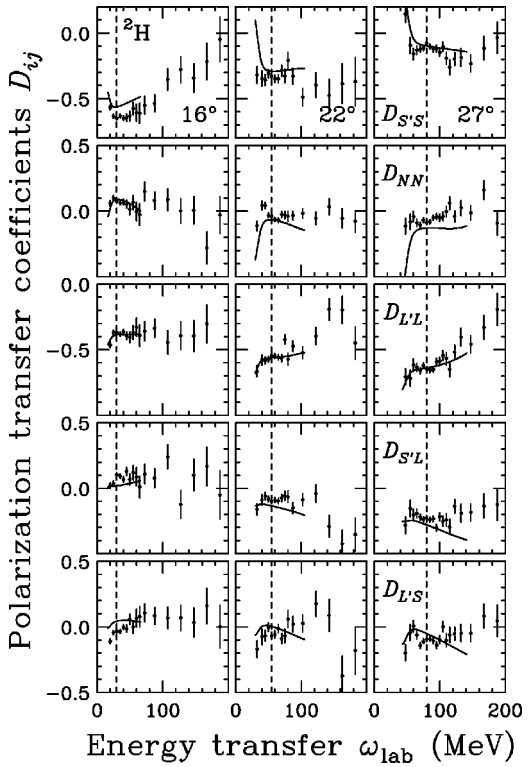

FIG. 2. Complete sets of polarization transfer coefficients for the ^{2}H(p,n) reaction at T_p=345 MeV and θ_{lab}=16°,22°, and 27°. The data are binned in 5–20 MeV steps, depending on their statistics. The notations of the curves are the same as those in Fig. 1.

^{12}C$(\vec{p},\vec{n})$ observables from the CD$_2(\vec{p},\vec{n})$ ones as

$$\sigma_{^2\mathrm{H}} = \frac{\sigma_{\mathrm{CD}_2} - \sigma_{\mathrm{C}}}{2}, \tag{3}$$

$$D_{^2\mathrm{H}} = \frac{D_{\mathrm{CD}_2} - f_{\mathrm{C}} D_{\mathrm{C}}}{1 - f_{\mathrm{C}}}, \tag{4}$$

where σ represents the cross section, D is one of the polarization observables, A_y, P, or D_{ij}, and $f_{\mathrm{C}}=\sigma_{\mathrm{C}}/\sigma_{\mathrm{CD}_2}$. The carbon fraction f_{C} was estimated by using the cross sections based on the nominal target thicknesses and integrated beam current. The relative normalization was adjusted to obtain the best subtraction of the prominent peak corresponding to the 4^- state at E_x=4.2 MeV in ^{12}N. The normalization factors varied from 0.98 to 1.02, which is most likely due to the uncertainty of the integrated beam current.

The cross sections, analyzing powers, and induced polarizations for the ^{2}H$(\vec{p},\vec{n})$ reaction at θ_{lab}=16°,22°, and 27° are presented in Fig. 1. The cross sections and analyzing powers are binned in 1 and 5 MeV intervals, respectively, while the induced polarizations are binned in 5–20 MeV intervals depending on their statistics. The shoulders of the quasielectric distributions at lower energy-transfer side are due to the $^1S_0$ final state interaction (FSI) of the residual two-proton system. The contribution of the FSI process decreases with increasing scattering angle. It should be noted that the analyzing power and induced polarization are in fairly good agreement with each other around the quasielastic peak. Thus, this reaction can be assumed as almost free $\vec{p}+n$ elastic scattering with little distortion effect.

Figure 2 shows complete sets of D_{ij} for the ^{2}H$(\vec{p},\vec{n})$ reaction at θ_{lab}=16°,22°, and 27°. The data at θ_{lab}=22° are published elsewhere [2]. The data herein are binned in 5–20 MeV intervals to reduce statistical fluctuations. The dotted vertical lines indicate the energy transfer for the free *np* scattering.

B. Comparison with PWIA calculations

The PWIA calculations for the ^{2}H(p,n) reaction were performed with the code developed by Itabashi, Aizawa, and Ichimura [4]. The initial deuteron and final *pp*-scattering wave functions are generated by the Reid soft core potential. Both *S* and *D* states are included in the deuteron, and the FSI process is included in the *pp* scattering. The *NN t*-matrix of Bugg and Wilkin [18] is used in the impulse approximation.

The solid curves in Figs. 1 and 2 represent the corresponding calculations. The calculations reproduce the cross sections reasonably well, but slightly underpredict the data near and below the quasielastic peak. The contribution of the

FSI process, while moderate at $\theta_{\rm lab}=16°$, decreases and appears as a shoulder of the quasielastic bump with increasing scattering angle. The PWIA results also reproduce the polarization observables reasonably well in the quasielastic region.

Recently Anderson *et al.* [1], and later Prout *et al.* [3] reported the cross section and complete set of polarization observables of the ^{2}H(p,n) reaction at 197 MeV. Their results are in good agreement with Faddeev-type calculations, in which the multiple scattering effects have been taken into account. This agreement and the present PWIA results certify that the reaction mechanisms are primarily direct at intermediate energies and the quasielastic process in the present momentum- and energy-transfer regions are well described by use of the impulse and optimal factorization approximations.

V. DISCUSSIONS

In this section, we deduce the experimental spin response functions, and compare them with theoretical and (e,e') response functions.

A. Coordinate system

The momentum transfer of the center-of-mass (c.m.) system is given by

$$\mathbf{q}=\mathbf{k}'-\mathbf{k}, \tag{5}$$

where $\mathbf{k}$ and $\mathbf{k}'$ are the momenta of the incident and outgoing nucleons in the c.m. frame, respectively. We use the c.m. coordinate system (q,n,p) defined as

$$\hat{\mathbf{q}}=\frac{\mathbf{q}}{|\mathbf{q}|}, \tag{6a}$$

$$\hat{\mathbf{n}}=\frac{\mathbf{k}\times\mathbf{k}'}{|\mathbf{k}\times\mathbf{k}'|}, \tag{6b}$$

$$\hat{\mathbf{p}}=\hat{\mathbf{q}}\times\hat{\mathbf{n}}. \tag{6c}$$

B. Reduction of experimental spin response functions

The unpolarized double differential cross section I in the laboratory frame is expressed as a sum of four polarized cross sections ID_i as

$$I=ID_0+ID_q+ID_n+ID_p, \tag{7}$$

where D_i are the polarization observables introduced by Bleszynski, Bleszynski, and Whitten [19], and they are related to the polarization transfer coefficients D_{ij} in the laboratory frame as [8]

$$D_0=\frac{1}{4}[1+D_{NN}+(D_{S'S}+D_{L'L})\cos\alpha_1+(D_{L'S}-D_{S'L})\sin\alpha_1], \tag{8a}$$

$$D_n=\frac{1}{4}[1+D_{NN}-(D_{S'S}+D_{L'L})\cos\alpha_1-(D_{L'S}-D_{S'L})\sin\alpha_1], \tag{8b}$$

$$D_q=\frac{1}{4}[1-D_{NN}+(D_{S'S}-D_{L'L})\cos\alpha_2-(D_{L'S}+D_{S'L})\sin\alpha_2], \tag{8c}$$

$$D_p=\frac{1}{4}[1-D_{NN}-(D_{S'S}-D_{L'L})\cos\alpha_2+(D_{L'S}+D_{S'L})\sin\alpha_2], \tag{8d}$$

where $\alpha_1\equiv\theta_{\rm lab}+\Omega$ and $\alpha_2\equiv 2\theta_p-\theta_{\rm lab}-\Omega$. The angle θ_p represents the angle between $\hat{\mathbf{k}}$ and $\hat{\mathbf{p}}$, and Ω is the the relativistic spin rotation angle defined in Ref. [8].

The polarized cross sections ID_i can be expressed in PWIA with eikonal and optimal factorization approximations as

$$ID_0=4K_{\rm lab}N_{\rm eff}(|A^\eta|^2R_0+|C_2^\eta|R_n), \tag{9a}$$

$$ID_q=4K_{\rm lab}N_{\rm eff}(|E^\eta|^2R_q+|D_1^\eta|R_p), \tag{9b}$$

$$ID_n=4K_{\rm lab}N_{\rm eff}(|B^\eta|^2R_n+|C_1^\eta|R_0), \tag{9c}$$

$$ID_p=4K_{\rm lab}N_{\rm eff}(|F^\eta|^2R_p+|D_2^\eta|R_q), \tag{9d}$$

where $K_{\rm lab}$ is the kinematical factor defined in Ref. [20], $N_{\rm eff}$ the effective neutron number, A^η–F^η the components of the optimal-frame NN t-matrix, and R_i the normalized spin response functions [2] determined by the nuclear intrinsic states. Note that the present $K_{\rm lab}$ is equal to $2(2J_A+1)CK$ in Ref. [2].

The contributions from D_1^η and D_2^η are very small compared with those from other components [2]. Thus the polarized cross sections, ID_q and ID_p, are almost directly related to the spin response functions, R_q and R_p, respectively. In general polarized cross sections, ID_0 and ID_n, are related to both the nonspin R_0 and spin-transverse R_n response functions. However, herein R_q and R_p may be approximated by the experimental spin-longitudinal and spin-transverse response functions, R_L and R_T, respectively.

C. Experimental spin response functions

Figure 3 shows the experimental spin-longitudinal and spin-transverse response functions, R_L and R_T, as functions of the mass difference $\omega_{\rm int}=m_{pp}-m_d$, where m_d is the deuteron mass and m_{pp} is the invariant mass of the final pp system. These response functions are deduced by using Eq. (9) with $N_{\rm eff}=1$. The solid curves in Fig. 3 represent the theoretical spin response functions calculated with the program code of Itabashi, Aizawa, and Ichimura [4]. The theoretical calculations can reproduce the shape of both spin-longitudinal and spin-transverse response functions very well, while the magnitude is somewhat underestimated, es-

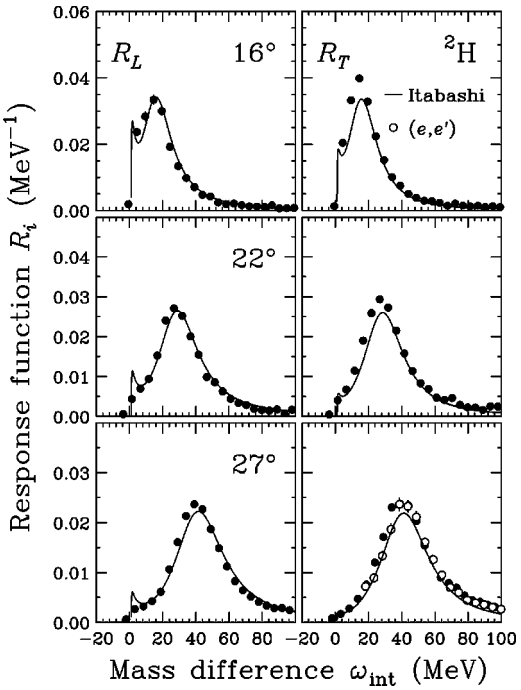

FIG. 3. Spin-longitudinal (left panels) and spin-transverse (right panels) response functions, R_L and R_T, for the ^{2}H(p,n) reaction at T_p=345 MeV and θ_{lab}=16°,22°, and 27°. The solid curves are the theoretical predictions with the Reid soft core potential. The open circles are R_T of the quasielastic electron scattering on ^{2}H [21].

pecially for R_T. The discrepancy between the experimental and theoretical results might be due to uncertainties in the reaction mechanisms, such as the multiple scattering effects. We note that the calculated R_L and R_T are smaller than the previously reported ones [2], since we corrected the program code and now the sum rules for R_L and R_T are satisfied in high accuracy.

The spin-transverse response function R_T of the quasielastic electron scattering on ^{2}H was reported by Dytman *et al.* [21]. The definition of R_T of the (e,e') scattering is described in Ref. [22], and the result at q=2.0 fm^{-1} is compared with the present $(\vec{p},\vec{n})$ spin-transverse response R_T in Fig. 3. The (e,e') spin-transverse response function agrees with the corresponding $(\vec{p},\vec{n})$ experimental R_T. The difference between the (e,e') and the theoretical R_T might be due to the contribution from the meson exchange current [21,23], which is neglected in the present analysis.

VI. SUMMARY AND CONCLUSION

The cross sections, analyzing powers, induced polarizations, and complete sets of polarization transfer coefficients for the quasielastic ^{2}H$(\vec{p},\vec{n})$ reaction were measured at T_p =345 MeV and θ_{lab}=16°,22°, and 27° ($q_{lab}\simeq$1.2,1.7, and 2.0 fm^{-1}). The data are compared with the PWIA calculations with the optimal factorization approximation. The theoretical calculations reproduce the experimental results well, which means that the impulse and optimal factorization approximations are good models for ^{2}H$(\vec{p},\vec{n})$ in the present momentum- and energy-transfer regions. This supports the assumption of dominant impulse processes used in the analysis of quasielastic $(\vec{p},\vec{n})$ reactions for nuclear targets.

The experimental spin-longitudinal and spin-transverse response functions are deduced from the spin-longitudinal and spin-transverse polarized cross sections, ID_q and ID_p, respectively. The consistency of the R_T values herein obtained via the (p,n) reaction with the corresponding R_T of the (e,e') scattering, supports the validity of the PWIA with the optimal factorization to deduce the (p,n) spin response functions. The theoretical calculations with the Reid soft core potential reproduce the R_L obtained via the (p,n) reaction, while they are slightly smaller than the R_T obtained via the (p,n) reaction and the (e,e') scattering. The small difference between the experimental and theoretical results could be due to the multiple scattering effects in the (p,n) reaction and the MEC effects in the (e,e') scattering.

ACKNOWLEDGMENTS

We are grateful to A. Itabashi for his helpful correspondence. We also thank Professor H. Toki for his continuous encouragement and the RCNP cyclotron crew for their efforts in providing a high quality polarized proton beam. The experiment was performed at RCNP under Program Number E131. This work was supported in part by the Grant-in-Aid for Scientific Research Nos. 14702005, 15340071, and 12640294 of the Ministry of Education, Culture, Sports, Science, and Technology of Japan.

[1] B. D. Anderson *et al.*, Nucl. Phys. **A631**, 752c (1998).
[2] T. Wakasa *et al.*, Phys. Rev. C **59**, 3177 (1999).
[3] D. L. Prout *et al.*, Phys. Rev. C **65**, 034611 (2002).
[4] A. Itabashi, K. Aizawa, and M. Ichimura, Prog. Theor. Phys. **91**, 69 (1994).
[5] A. Picklesimer, P. C. Tandy, R. M. Thaler, and D. H. Wolfe, Phys. Rev. C **30**, 1861 (1984).
[6] S. A. Guyrvitz, Phys. Rev. C **33**, 422 (1986).
[7] X. Q. Zhu, N. Mobed, and S. S. M. Wong, Nucl. Phys. **A466**, 623 (1987).
[8] M. Ichimura and K. Kawahigashi, Phys. Rev. C **45**, 1822 (1992).
[9] J. B. McClelland *et al.*, Phys. Rev. Lett. **69**, 582 (1992).
[10] X. Y. Chen *et al.*, Phys. Rev. C **47**, 2159 (1993).
[11] T. N. Taddeucci *et al.*, Phys. Rev. Lett. **73**, 3516 (1994).
[12] C. Hautala *et al.*, Phys. Rev. C **65**, 034612 (2002).
[13] H. Sakai, H. Okamura, H. Otsu, T. Wakasa, S. Ishida, N. Sakamoto, T. Uesaka, Y. Satou, S. Fujita, and K. Hatanaka, Nucl. Instrum. Methods Phys. Res. A **369**, 120 (1996).
[14] H. Sakai, H. Okamura, S. Ishida, K. Hatanaka, and T. Noro, Nucl. Instrum. Methods Phys. Res. A **320**, 479 (1992).
[15] T. Wakasa *et al.*, Nucl. Instrum. Methods Phys. Res. A **404**,

355 (1998).
[16] K. Hatanaka, K. Takahisa, H. Tamura, M. Sato, and I. Miura, Nucl. Instrum. Methods Phys. Res. A **384**, 575 (1997).
[17] T. N. Taddeucci *et al.*, Phys. Rev. C **41**, 2548 (1990).
[18] D. V. Bugg and C. Wilkin, Nucl. Phys. **A467**, 575 (1987).
[19] E. Bleszynski, M. Bleszynski, and J. C. A. Whitten, Phys. Rev. C **26**, 2063 (1982).
[20] K. Kawahigashi, K. Nishida, A. Itabashi, and M. Ichimura, Phys. Rev. C **63**, 044609 (2001).
[21] S. A. Dytman, A. M. Bernstein, K. I. Blomqvist, T. J. Pavel, B. P. Quinn, R. Altemus, J. S. McCarthy, G. H. Mechtel, T. S. Ueng, and R. R. Whitney, Phys. Rev. C **38**, 800 (1988).
[22] K. Nishida and M. Ichimura, Phys. Rev. C **51**, 269(1995).
[23] B. P. Quinn *et al.*, Phys. Rev. C **37**, 1609 (1987).